文章编号 2097-1842(2026)02-0382-13

Gold nanowire bias-core PCF-SPR temperature and refractive index sensing

HOU Shang-lin[1*], DONG Jie[1], YANG Xu-dong[1], LIU Qing-min[1],
XIE Cai-jian[2], WU Gang[1], YAN Zu-yong[1]
（1. *School of Science*, *Lanzhou University of Technology*, *Lanzhou* 730050, *China*;
2. *College of Information Science and Technology*, *Zhongkai University of Agriculture and Engineering*, *Guangzhou* 510225, *China*）
* *Corresponding author*, *E-mail*: *houshanglin@vip.*163.*com*

Abstract: To address the challenges of complex metallic film coating processes and low integration in single-parameter detection for existing photonic crystal fiber surface plasmon resonance (PCF-SPR) sensors, a dual-parameter sensor based on gold nanowire-integrated bias-core PCF-SPR is proposed. Unlike conventional in-hole coatings or metallic film structures, the gold nanowires are directly attached to the fiber cladding via chemical vapor deposition (CVD), eliminating uneven coating issues and significantly simplifying fabrication. By optimizing the asymmetric bias-core fiber structure and leveraging the strong localized field enhancement of gold nanowires, the sensor achieves high-sensitivity synchronous detection of temperature (25−60 °C) and refractive index (1.31−1.40) in dual-polarization modes. The simulation results demonstrate that the x-polarization mode can achieve 1.31−1.40 refractive index detection with maximum wavelength sensitivity and amplitude sensitivity of 14 800 nm/RIU and −1 724.25 RIU^{-1}, and maximum refractive index resolution of 6.75×10^{-6} RIU. The y-polarization mode achieves refractive index detection range of 1.34−1.40, and the maximum wavelength sensitivity and amplitude sensitivity are 28 400 nm/RIU and −1 298.93 RIU^{-1}, and the maximum refractive index resolution is 3.52×10^{-6} RIU. For temperature sensing, the sensor exhibits a wavelength sensitivity of 7.8 nm/°C and a high resolution of 1.38×10^{-6} °C over the range of 25−60 °C. This design synergizes gold nanowires and the bias-core architecture to simplify fabrication while enabling multi-parameter detection. The proposed sensor offers new insights for integrated applications in biochemical monitoring, environmental sensing, and related fields.

Key words: photonic crystal fiber; surface plasmon resonance; gold nanowires; temperature; sensor

收稿日期:2025-07-04; **修订日期**:2025-07-21

基金项目:国家自然科学基金(No. 61665005); 甘肃省自然科学基金(No. 24JRRA208)
Supported by National Natural Science Foundation of China (No. 61665005); Natural Science Foundation of Gansu Province (No. 24JRRA208)

金纳米线偏置芯光子晶体光纤表面等离子体共振温度与折射率传感

侯尚林[1]*, 董　洁[1], 杨旭东[1], 刘庆敏[1], 谢彩健[2], 武　刚[1], 晏祖勇[1]
（1. 兰州理工大学 理学院, 甘肃 兰州 730050;
2. 仲恺农业工程学院 信息科学与技术学院, 广东 广州 510225）

摘要: 针对现有光子晶体光纤表面等离子体共振(PCF-SPR)传感器存在的金属薄膜涂覆工艺复杂、单参数检测集成度低等问题, 本文提出一种基于金纳米线集成偏置芯 PCF-SPR 的双参数传感器。该传感器突破传统孔内镀膜或金属薄膜结构, 通过化学气相沉积(CVD)将金纳米线直接附着于光纤包层, 避免了镀膜不均问题并显著简化制备工艺。通过优化非对称偏置芯光纤结构并利用金纳米线的强局域场增强效应, 该传感器在双偏振模式下实现了温度(25~60 °C)与折射率(1.31~1.40)的高灵敏度同步检测。仿真实验表明: x 偏振模式可实现 1.31~1.40 折射率检测, 最大波长灵敏度与振幅灵敏度分别达 14 800 nm/RIU 和−1 724.25 RIU^{-1}, 最高折射率分辨率为 6.75×10^{-6} RIU; y 偏振模式折射率检测范围达 1.34~1.40, 最大波长灵敏度与振幅灵敏度分别为 28 400 nm/RIU 和−1 298.93 RIU^{-1}, 最高折射率分辨率为 3.52×10^{-6} RIU。在 25~60 °C 温度传感中, 传感器表现出 7.8 nm/°C 的波长灵敏度与 1.38×10^{-6} °C 的高分辨率。该设计通过金纳米线与偏置芯结构的协同作用, 在简化制备工艺的同时实现了多参数检测, 为生化监测、环境传感等领域的集成化应用提供了新思路。

关　键　词: 光子晶体光纤; 表面等离子体共振; 金纳米线; 温度; 传感器
中图分类号: TN29　　**文献标志码:** A　　**doi:** 10.37188/CO.EN-2025-0034　　**CSTR:** 32171.14.CO.EN-2025-0034

1　Introduction

Surface Plasmon Resonance (SPR) is a physical phenomenon generated by the coupling of incident light waves with the collective oscillation of free electrons on the metal surface[1]. When a light wave excites a surface plasmon wave at a metal-dielectric interface (e.g., a gold or silver thin film), its resonant wavelength or angle is highly sensitive to the change of refractive index of the surrounding medium, which makes it a core principle of high sensitivity sensing technology[2]. Among them, gold nanowires have demonstrated remarkable advantages in the field of SPR sensors due to their unique geometric properties[3]. With high specific surface area and strong localized field enhancement effects, gold nanowires can significantly enhance the interaction efficiency between light and metal surfaces, thereby effectively improving sensor sensitivity[4-5]. In recent years, optical fibers have gained widespread application in SPR sensing due to their excellent electromagnetic interference resistance, corrosion resistance, and miniaturization characteristics[6-7]. Among various fiber-optic SPR sensors, photonic crystal fiber-based surface plasmon resonance (PCF-SPR) sensors have emerged as an ideal platform for current SPR sensing technology research, owing to their unique advantages in flexible light-field manipulation and structural design freedom[8-10].

Since Hassani and Skorobogatiy pioneered the first PCF-SPR sensor in 2006[11], this technology has achieved remarkable advancements in both sensing performance and device configuration. In the early days, the PCF-SPR sensor was mainly prepared by coating the inner wall of air hole with metal film[12-13]. In this technology, a metal film structure is formed on the inner surface of micron-sized air holes by chemical coating or chemical vapor deposition[14], and then a liquid sample to be measured is injected to stimulate the surface plasmon resonance

effect. However, the uniformity control of metal thin film in micro-scale confined space and the compatibility between metallization and liquid filling process significantly increase the difficulty and process complexity of sensor preparation. In comparison with conventional PCF-SPR sensors based on internal plasma coating[15-17] and open-loop channel coating processes[18-20], nanowire-integrated PCF-SPR sensors[21-24] fully exploit the unique advantages of nano-plasmonic structural materials. This innovative approach directly assembles nanowires on the outer surface of fiber cladding, effectively addressing the long-standing uniformity control challenges associated with traditional planar metal thin-film deposition techniques. Recent years have witnessed significant breakthroughs in structural innovation and performance enhancement for gold-nanowire-based PCF-SPR sensors. Various novel structural designs, particularly D-shaped and eccentric-core configurations[25-26], demonstrate substantially improved sensing performance in applications such as temperature sensing and refractive index detection. For example, in 2020, Wang *et al*.[27] developed a PCF-SPR sensor with double gold nanowires in series structure, which can realize wide-range detection of low refractive index range of 1.13−1.35 in near infrared region. The simulation results show that the sensor can achieve a maximum sensitivity of 17 500 nm/RIU and a resolution of 5.71×10^{-6} RIU. In 2023, He *et al*.[28] developed a new type of ring-core PCF-SPR sensor. The wavelength sensitivity of 40 000 nm/RIU and the amplitude sensitivity of 2 141 RIU^{-1} are realized in the wide refractive index range of 1.13−1.45, and the resolution reaches 2.5×10^{-6} RIU. In 2024, Liu *et al*.[29] developed a gold nanowire integrated eccentric PCF-SPR sensor, which can achieve the highest wavelength sensitivity of 51 200 nm/RIU and amplitude sensitivity of −1 248.5 RIU^{-1} in the refractive index range of 1.34−1.39.

However, most currently available PCF-SPR sensors capable of temperature and refractive index detection are limited to single-parameter measurements, which often fail to meet practical application requirements. With advancements in PCF design and fabrication technologies, researchers have developed various PCF-SPR sensor configurations that enable simultaneous multi-parameter detection of analyte refractive index, temperature, magnetic field, and other physical quantities. For example, in 2024, Liu *et al*.[30] designed a two-parameter sensor for SPR of anti-resonance optical fiber to detect magnetic field and temperature simultaneously. The simulation results show that the maximum sensitivity is 500 pm/Oe when the magnetic field is between 50 and 130 Oe. In the temperature range of 20−30 °C, the maximum wavelength sensitivity is 10.8 nm/°C. In 2025, Xu *et al*.[31] proposed a PCF-SPR sensor which can be used to detect three parameters of magnetic field, temperature and refractive index. The simulation results show that the temperature detection range of the sensor is 0 to 100 °C, and the wavelength sensitivity is 6.6 nm/°C. The detection range of magnetic field is 0 to 100 mT, and the wavelength sensitivity is 0.75 nm/mT. The detection range of refractive index is 1.410 to 1.435, and the wavelength sensitivity is 29 800 nm/RIU. Although these sensors provide innovative approaches and insights for realizing multi-parameter SPR sensing, several technical challenges remain to be addressed. Notably, the mechanical strength of D-shaped PCFs is significantly compromised by the required side-polishing process, while hollow-core anti-resonant fibers exhibit inherent structural complexity that poses fabrication difficulties.

In order to solve the above problems, a bias-core PCF sensor based on gold nanowire SPR is proposed in this paper. On the premise of ensuring the mechanical strength of optical fiber, the distance between fiber core and plasma material layer is shortened by combining the circular eccentric PCF structure with nanowire plasma material, which simplifies the preparation process and solves the problem of uneven coating. Therefore, this sensor

has practical significance and great application potential in refractive index monitoring and related physical quantity sensing.

2 Theoretical analysis

The two-dimensional cross-section of the PCF-SPR sensor with a single gold nanowire core proposed in this paper is shown in Fig. 1(a) (color online). In the PCF of this sensor, air holes are arranged periodically on the silica. Three large air holes are used to reduce the average refractive index in their vicinity, resulting in energy leakage only through the sensing channel at the top of the core. Since the average refractive index in the vicinity of the small air holes is closer to the refractive index of the core, the energy is more likely to be transferred to the sensing region through the energy leakage channel formed by the small air holes. The energy leakage from the core to the sensing region can be controlled by adjusting the air holes. For optimum sensing performance, the radii of the large and small air holes in the PCF are set to d_1=1.2 μm and d_2=0.7 μm, and the aperture period is set to $\Lambda=\sqrt{2}\times P$ μm with P=1.7. The role of the perfect matching layer (PML) is to absorb the radiant energy. To ensure the practicality of the sensor and a loss spectrum with narrow loss peaks, the sensor uses gold nanowires with a radius of d_3=0.35 μm as SPRs. The three-dimensional structure and three-dimensional longitudinal perspective view of the sensor are shown in Figs. 1(b) and 1(c) (color online), respectively.

The manufacturing process of the proposed PCF-SPR sensor includes the following steps. Firstly, the PCF without gold wires is fabricated at a high temperature by using the conventional stacking and fusing of capillary arrays[32]. Next, the gold nanowires are prepared[33] by chemical vapor deposition (CVD), and the prepared gold nanowires only need to be attached to the outside of the cladding to realize sensing. Thirdly, the gold nanowires are embedded by the spliced-fiber pressure-filling technique or the high-pressure chemical deposition techniques[34]. Finally, the PCF with embedded gold wires is stretched under the appropriate pressure, temperature conditions to realize the proposed sensor.

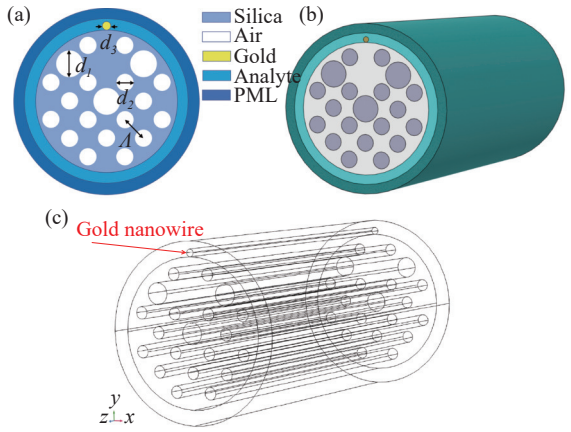

Fig. 1　Gold nanowire biased core PCF-SPR sensor. (a) Two-dimensional cross-sectional diagram; (b) three-dimensional structure; (c) three-dimensional perspective view

The material of the PCF-SPR sensor is silica, whose refractive index can be defined by Sellmeier equation[35]

$$n^2(\lambda)=1+\frac{A_1\lambda^2}{\lambda^2-B_1^2}+\frac{A_2\lambda^2}{\lambda^2-B_2^2}+\frac{A_3\lambda^2}{\lambda^2-B_3^2}\quad,\quad(1)$$

where λ is the wavelength of incident light, A_1=0.696 166 3, A_2=0.407 942 6, A_3=0.897 479 4, B_1=0.068 404 3 μm, B_2=0.116 241 4 μm, B_3=9.896 161 0 μm.

In SPR sensing systems, the interaction between gold nanowires and the fiber evanescent field is fundamentally achieved through phase-matched coupling between propagating surface plasmon polaritons (SPPs) and the fiber guide mode. The high aspect ratio of the nanowires enhances coupling efficiency through three key effects: reducing SPP propagation loss, generating strong longitudinal field localisation, and increasing evanescent field overlap. These characteristics are closely related to the complex permittivity function $\varepsilon(\omega)=\varepsilon_1(\omega)+i\varepsilon_2(\omega)$ of gold, where the imaginary part ε_2 determ-

ines optical loss, and the real part ε_1 dominates the SPP dispersion characteristics. This highly efficient light-plasmon coupling mechanism forms the physical foundation for the enhanced sensitivity of nanowire SPR sensors. Furthermore, the dielectric constant of gold can be expressed by the Drude-Lorentz model[36]

$$\varepsilon_{\mathrm{Au}}=\varepsilon_{\infty}-\frac{\omega_{\mathrm{D}}^{2}}{\omega(\omega+j\gamma_{\mathrm{D}})}-\frac{\Delta\varepsilon\Omega_{\mathrm{L}}}{(\omega^{2}-\Omega_{\mathrm{L}}^{2})+j\Gamma_{\mathrm{L}}\omega}, \quad (2)$$

where $\varepsilon_{\infty}=5.967\,3$ is the dielectric constant of gold at high frequencies, ω_{D} and γ_{D} are the plasma frequency and damping frequency, with values $\omega_{\mathrm{D}}/2\pi=2\,113.6$ THz, $\gamma_{\mathrm{D}}/2\pi=15.92$ THz. $\Delta\varepsilon$ is a weight factor of size 1.09, Γ_{L} and Ω_{L} are the frequency and spectral width of the Lorentz oscillator with values $\Gamma_{\mathrm{L}}/2=104.86$ Hz and $\Omega_{\mathrm{L}}/2\pi=650.07$ THz, respectively.

When part of the energy in the fiber leaks into the sensing region, the fundamental mode gradually couples with the SPP mode, and as the coupling progresses, a clear absorption peak appears on the output spectrum. While the loss peak reaches the peak, the fundamental mode and SPP mode also achieve the most complete coupling.

Confinement loss is an important parameter used to evaluate the performance of the PCF-SPR sensor, which can be calculated by Eq. (3)[37]

$$CL=8.686\times\frac{2\pi}{\lambda}\mathrm{Im}(n_{\mathrm{eff}})\times10^{4}\ (\mathrm{dB/cm}) \quad , \quad (3)$$

where $\mathrm{Im}(n_{\mathrm{eff}})$ denotes the imaginary part of the effective refractive index of the mode.

The wavelength sensitivity of the sensor is related to the wavelength and refractive index, which is defined as[38]

$$S_{\lambda}(\lambda)=\frac{\Delta\lambda_{\mathrm{peak}}}{\Delta n_{\mathrm{a}}}\ (\mathrm{nm/RIU}) \quad , \quad (4)$$

where $\Delta\lambda_{\mathrm{peak}}$ is the offset of the resonance wavelength, and Δn_{a} denotes the change in refractive index of the medium to be measured.

Resolution is an important parameter for evaluating the performance of refractive index sensors, which can be expressed as[39]

$$R=\frac{\Delta n_{\mathrm{a}}\times\Delta\lambda_{\mathrm{min}}}{\Delta\lambda_{\mathrm{peak}}} \quad , \quad (5)$$

where $\Delta\lambda_{\mathrm{min}}$ is the highest resolution of the laboratory spectrum, which is typically 0.01 nm.

The quality factor, defined as the ratio of wavelength sensitivity to full width at half height, is another key parameter for evaluating the performance of the PCF-SPR sensor and can be expressed as[40]

$$FOM=\frac{S_{\lambda}(\lambda)}{FWHM} \quad . \quad (6)$$

The sensing performance of the PCF-SPR sensor can also be evaluated in terms of amplitude sensitivity, which can be defined as[41]

$$S(\mathrm{RIU}^{-1})=-\frac{1}{\alpha(\lambda,n_{\mathrm{a}})}\frac{\partial\alpha(\lambda,n_{\mathrm{a}})}{\partial n_{\mathrm{a}}} \quad , \quad (7)$$

where $\alpha(\lambda,n_{\mathrm{a}})$ is the total confinement, ∂n_{a} is the amount of change in the refractive index of the object to be measured, and $\partial\alpha(\lambda,n_{\mathrm{a}})$ is the difference in resonance intensities of neighboring loss spectra caused by the change in the refractive index of the object to be measured.

3 Results and analysis

3.1 Characterization of sensor loss spectra

The confinement loss spectra and the effective refractive index curves of the fundamental mode and SPP mode as a function of wavelength are shown Fig. 2 (color online). The black curve is the confinement loss of the fundamental mode, and the blue and red curves indicate the real part of the effective mode refractive indices of the SPP mode and the fundamental mode, respectively. It can be seen from the figure that the real part of the effective refractive index of the fundamental mode and SPP mode decreases with the increase of wavelength. However, due to the difference in the rate of decrease of the real part of the effective refractive indices of the two modes, there is an intersection of

the blue and red curves as the wavelength increases. The real parts of the effective refractive index curves of the x-polarized and y-polarized fiber fundamental mode and the SPP mode intersect at wavelengths of 1 005 nm and 1 055 nm, respectively. It can be found that the intersection point of the two curves corresponds to the same wavelength as the confinement peak of the fundamental mode confinement peak. This wavelength is referred to as the resonance wavelength and the intersection point is referred to as the phase matching point.

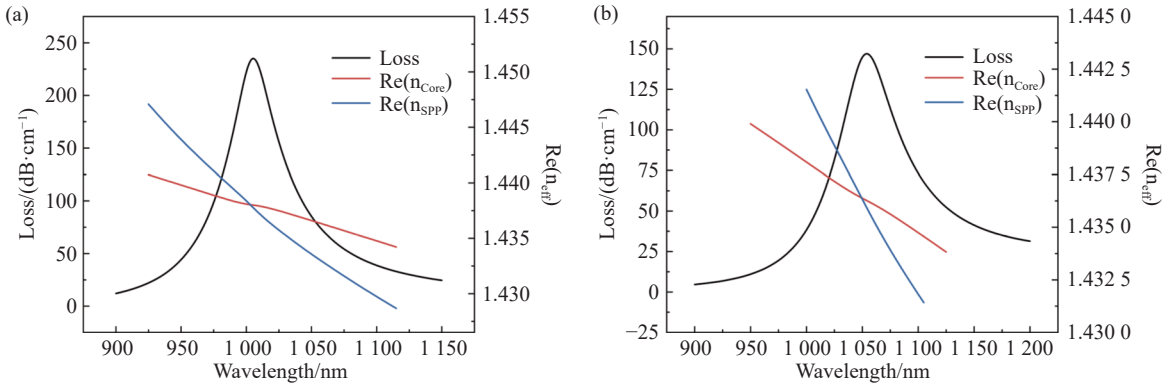

Fig. 2　Confinement loss spectral and effective refractive index curves of the fundamental mode and SPP mode as a function of wavelength for (a) x-polarized fundamental mode and (b) y-polarized fundamental mode

The electric field distributions of the x-polarized fundamental mode and y-polarized fundamental mode at three different wavelengths are shown in Fig. 3 (color online).

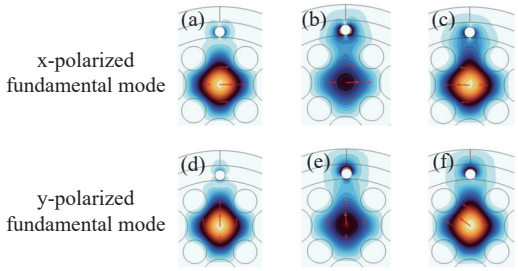

Fig. 3　Electric field distributions of *x*- and *y*-polarized fundamental modes at different wavelengths. (a) (d) 900 nm; (b) (e) 1 055 nm; (c) (f) 1 200 nm

For the x-polarized fundamental mode, the electric field distributions at 900 nm, 1 005 nm, and 1 200 nm are shown in Figs. 3(a), 3(b), and 3(c), respectively. The energy leakage of the fundamental mode is the largest at the resonant wavelength of 1 005 nm, which also corresponds to the maximum loss of the fundamental mode outside the wavelength in Fig. 2(a). Similarly, Figs. 3(d), 3(e), and 3(f) show the electric field distributions of the y-polarized fundamental mode at 900 nm, 1 055 nm, and 1 200 nm, respectively. Among them, the energy leakage of y-polarized fundamental mode with resonance wavelength of 1 055 nm is the most significant when the confinement loss reaches the peak. The effect of air holes on energy leakage can be seen from the electric field distribution in Fig. 3, due to the fact that the introduction of air holes reduces the average refractive index of the medium around them, thus inhibiting the transfer of energy in the fiber core.

3.2　Characterization of the sensor sensing

The confinement spectra of the fundamental mode of the gold nanowire-based PCF-SPR sensor at different analyte refractive indices is shown in Fig. 4 (color online). It can be seen from Fig. 4(a) that the refractive index detection range of the sensor in the x-polarization mode is 1.31−1.40. As the refractive index increases, the loss in x-polarized mode gradually increases and the resonance wavelength is red-shifted. This is because the increase of the refractive index of the measured substance will reduce the refractive index difference between the fiber core and the sensing area. At this time, longer wavelength light is needed to stimulate

the SPR effect. It can be seen from Fig. 4(b) that the detection range of refractive index of the sensor in y-polarization mode is 1.34−1.40. As the refractive index increases, a gradual decrease in the peak loss and a red shift of the resonance wavelength also occurs. It can be seen from Eq. (4) that when the refractive index change is fixed at 0.01, the larger the resonance wavelength shift, the higher the sensitivity of the sensor.

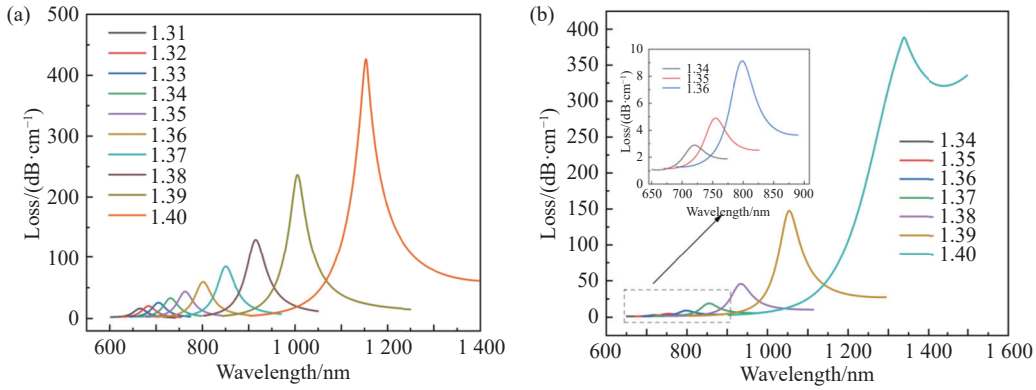

Fig. 4 Confinement spectra of (a) x-polarized fundamental mode and (b) y-polarized fundamental mode for different refractive indices

The variation of amplitude sensitivity with increasing wavelength at different refractive indices for both polarization modes is shown in Fig. 5 (color online). As the refractive index of the material to be measured increases, the maximum amplitude sensitivities of both x-polarization and y-polarization modes keep increasing. At the same refractive index of the material to be measured, the amplitude sensitivities corresponding to x-polarization and y-polarization modes firstly decrease and then increase with the increase of wavelength and finally tend to stabilize. The maximum amplitude sensitivities corresponding to x-polarization and y-polarization modes are −1 724.3 RIU^{-1} and −1 298.9 RIU^{-1}, respectively.

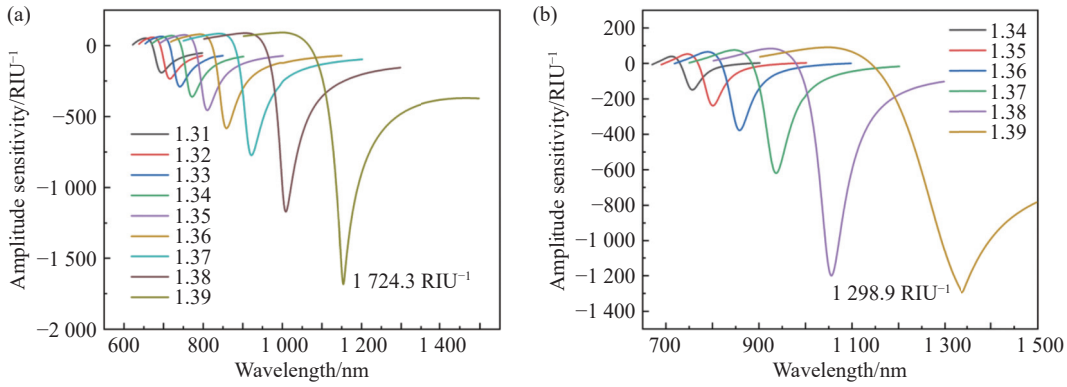

Fig. 5 Variation of amplitude sensitivity with wavelength for (a) x-polarized fundamental mode and (b) y-polarized fundamental mode at different refractive indices

The effect of the variation of the refractive index of the object to be measured on the resonance wavelength of the two polarization modes is shown in Fig. 6 (color online). Polynomials were fitted to the refractive index of the object to be measured and its corresponding resonance wavelengths in the x-polarized and y-polarized fundamental modes, respectively, and the slopes of the points on the fitted curves indicate the wavelength sensitivity of this gold nanowire bias-core SPR fiber sensor. The res-

ults show that the R^2 of the x-polarized and y-polarized fundamental mode are 0.997 48 and 0.992 39, respectively, which indicates that the sensor has a good refractive index sensing response in both polarization modes.

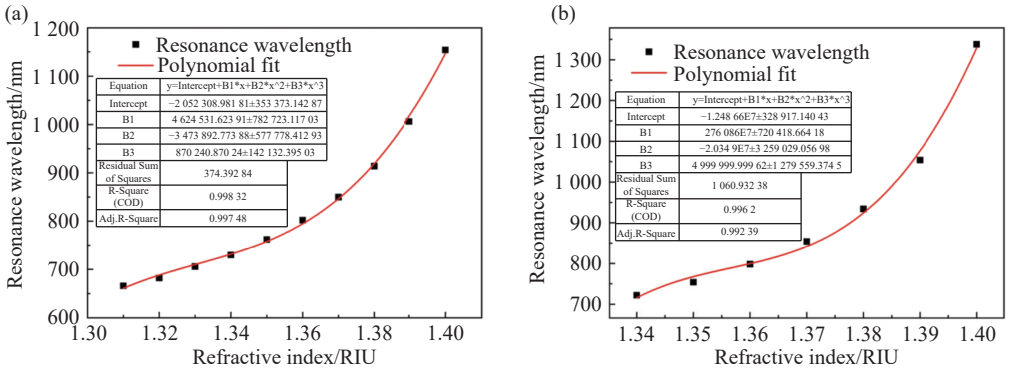

Fig. 6　Variation of resonance wavelength with refractive index in (a) x-polarized fundamental mode and (b) y-polarized fundamental mode

The wavelength sensitivity, amplitude sensitivity and resolution of the gold nanowire-based PCF-SPR refractive index sensor are summarized in Table 1. Among them, the refractive index detection range, maximum wavelength sensitivity, amplitude sensitivity and refractive index resolution of the corresponding sensor in x-polarization mode are 1.31−1.40, 14 800 nm/RIU, −1 724.25 RIU^{-1} and 6.7×10^{-6} RIU, respectively. The refractive index detection range, maximum wavelength sensitivity, amplitude sensitivity and refractive index resolution of the corresponding sensor in y-polarization mode are 1.34−1.40, 28 400 nm/RIU, −1 298.93 RIU^{-1} and 3.52×10^{-6} RIU, respectively. Compared with the performance of the sensor in y-polarization mode, the wavelength sensitivity and resolution of the sensor in x-polarization mode are lower, but its refractive index detection range is wider, and its amplitude sensitivity is higher.

Tab. 1　Performance of single gold nanowire bias-core PCF-SPR refractive index sensor

Refractive index of the substance to be measured (RIU)	Polarization type	Wavelength sensitivity (nm/RIU)	Amplitude sensitivity (RIU^{-1})	Resolution (RIU)
1.31	*x*-polarization	1 600	−192.57	6.25×10^{-5}
	y-polarization	–	–	–
1.32	*x*-polarization	2 400	−235.16	4.17×10^{-5}
	y-polarization	–	–	–
1.33	*x*-polarization	2 400	−291.80	4.17×10^{-5}
	y-polarization	–	–	–
1.34	*x*-polarization	3 200	−362.15	3.13×10^{-5}
	y-polarization	3 200	−150.50	3.13×10^{-5}
1.35	*x*-polarization	4 000	−459.04	2.50×10^{-5}
	y-polarization	4 400	−240.16	2.27×10^{-5}
1.36	*x*-polarization	4 800	−586.60	2.08×10^{-5}
	y-polarization	5 600	−380.72	1.79×10^{-5}
1.37	*x*-polarization	6 400	−778.15	1.56×10^{-5}
	y-polarization	8 000	−622.04	1.25×10^{-5}

续表 1

Refractive index of the substance to be measured (RIU)	Polarization type	Wavelength sensitivity (nm/RIU)	Amplitude sensitivity (RIU^{-1})	Resolution (RIU)
1.38	*x*-polarization	9200	−1176.40	1.09×10^{-5}
	y-polarization	12000	−1202.94	8.33×10^{-6}
1.39	*x*-polarization	14800	−1724.25	6.75×10^{-6}
	y-polarization	28400	−1298.93	3.52×10^{-6}
1.40	*x*-polarization	–	–	–
	y-polarization	–	–	–

3.3 Application of sensor in temperature detection

In recent years, PCF-SPR sensors have made significant progress in the fields of temperature, stress and biochemical detection. In order to verify the performance of the gold nanowire bias-core PCF-SPR sensors designed in this paper for practical applications, the next step is to focus on its characteristics in temperature sensing.

The refractive index of a mixture of alcohol and chloroform can be expressed as[42]

$$\begin{aligned} n_{\mathrm{m}} = & x\% \times [n_{\mathrm{ethanol}}|T = \\ & 20^{\circ}\mathrm{C} + \frac{dn_{\mathrm{ethanol}}}{dT} \times (T-20)] + \\ & (100-x)\% \times [n_{\mathrm{chloroform}}|T = \\ & 20^{\circ}\mathrm{C} + \frac{dn_{\mathrm{chloroform}}}{dT} \times (T-20)] \quad , \end{aligned} \tag{8}$$

where n_{m} is the refractive index of the mixture; x% and (100−x)% are the proportion of alcohol and chloroform, respectively; dn/dT indicates the thermo-optic coefficient, which is -3.94×10^{-4}/°C and -6.328×10^{-4}/°C for alcohol and chloroform, respectively. At 20 °C, the refractive indices of alcohol and chloroform are 1.36048 and 1.43136, respectively. Since the thermo-optic coefficient of optical fiber is much smaller than that of alcohol and chloroform, the effect of temperature on the PCF can be neglected. The ratio of alcohol to chloroform is set to 1∶1, and considering the boiling points of alcohol and chloroform, the upper limit for the sensor to measure their mixtures is 60 °C. When the ratio of alcohol to chloroform is 1∶1, the refractive index of the mixture as a function of temperature is shown in Fig. 7.

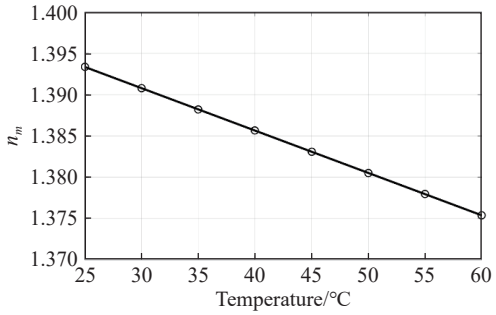

Fig. 7 Variation of refractive index of alcohol-chloroform mixtures with temperature

It can be seen from Fig. 7 that the refractive index of the alcohol-chloroform mixtures decreases gradually with an increasing temperature. The loss spectra of the two polarization modes at different temperatures are shown in Fig. 8 (color online). As can be seen from Fig. 8, as the temperature increases from 25 °C to 60 °C, the loss peak gradually decreases and the resonance wavelength is blue-shifted. This is because the rising temperature reduces the refractive index of the alcohol-chloroform mixture, and the decrease of the refractive index affects the coupling between the fundamental mode and the SPP mode, which ultimately leads to the decrease of the peak loss and the blue shift of the resonance wavelength. Since the sensitivity of the temperature sensor is related to the resonance wavelength offset and the temperature change, both of which are 5 °C, the sensing performance can be calculated by studying the resonance wavelength blueshift. It can also be noticed from the figure that the FWHM of the loss profile of the x-polarized sensor is smaller than that of the sensor in y-polarized mode.

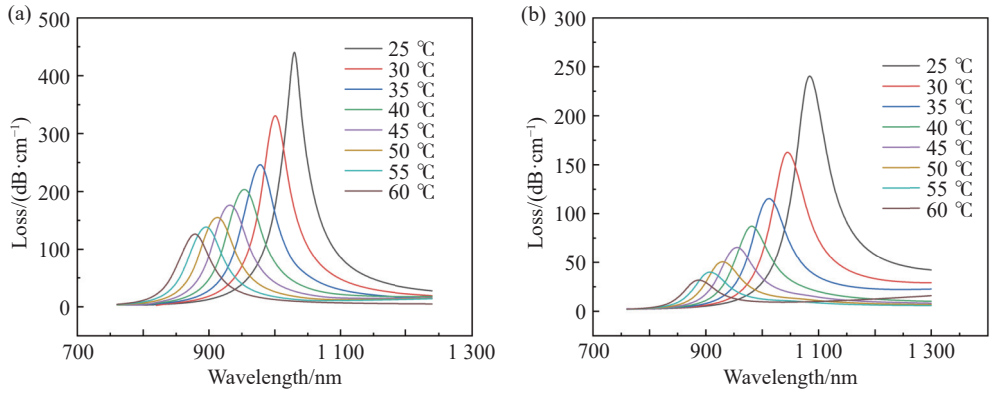

Fig. 8　Confinement spectra of (a) x-polarized fundamental mode and (b) y-polarized fundamental mode at different temperatures

The polynomial fit of the temperature to its corresponding resonance wavelength is shown in Fig. 9 (color online). The resonance wavelength decreases as the temperature increases. The slope of each point in the graph represents the wavelength sensitivity at that point. When the temperature is increased from 25 °C to 60 °C in steps of 5 °C, the decreases of resonance wavelengths are 28 nm, 25 nm, 27 nm, 18 nm, 19 nm, 18 nm, 16 nm for x-polarization, and 39 nm, 35 nm, 30 nm, 27 nm, 24 nm, 22 nm, 20 nm for y-polarization, respectively. The fitting results show that the x-polarized mode and y-polarized mode have R^2 of 0.999 28 and 0.999 72, respectively, which indicates that the sensors of these two polarization modes have good temperature sensing response.

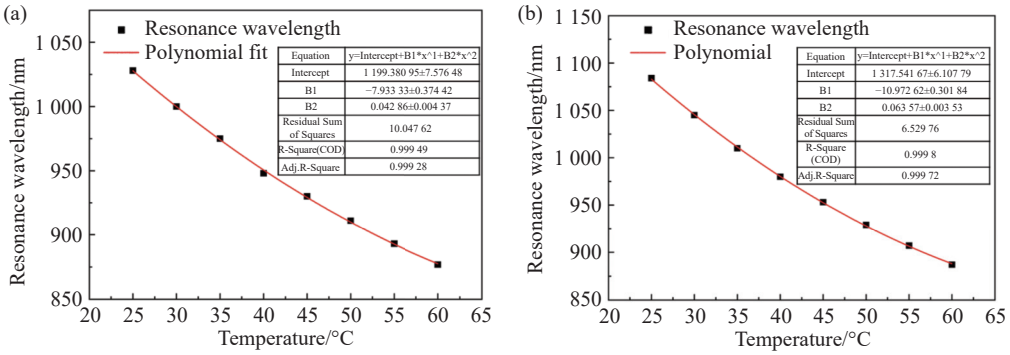

Fig. 9　Variation of resonance wavelength with temperature in (a) *x*-polarization mode and (b) *y*-polarization mode

The wavelength sensitivity and resolution of the gold nanowire bias-core PCF-SPR temperature sensor are summarized in Table 2. The temperature detection range, maximum wavelength sensitivity and temperature resolution of the sensor in x-polarized mode are 25−60 °C, 5.6 nm/°C and 1.79×10^{-2} °C, respectively. The temperature detection range, maximum wavelength sensitivity and temperature resolution of the sensor in y-polarized mode are 25−60 °C, 7.8 nm/°C and 1.38×10^{-2} °C, respectively.

Tab. 2　Temperature sensing performance of single gold nanowire bias-core PCF-SPR sensors

Temperature to be measured (°C)	Polarization type	Wavelength sensitivity (nm/°C)	Resolution (°C)
25	*x*-polarization	5.6	1.79×10^{-2}
	y-polarization	7.8	1.28×10^{-2}
30	*x*-polarization	5	2×10^{-2}
	y-polarization	7	1.43×10^{-2}
35	*x*-polarization	5.4	1.85×10^{-2}
	y-polarization	6	1.67×10^{-2}
40	*x*-polarization	3.6	2.78×10^{-2}
	y-polarization	5.4	1.85×10^{-2}

续表 2

Temperature to be measured (°C)	Polarization type	Wavelength sensitivity (nm/°C)	Resolution (°C)
45	*x*-polarization	3.8	2.63×10^{-2}
	y-polarization	4.8	2.08×10^{-2}
50	*x*-polarization	3.6	2.78×10^{-2}
	y-polarization	4.4	2.27×10^{-2}
55	*x*-polarization	3.2	3.13×10^{-2}
	y-polarization	4	2.5×10^{-2}
60	*x*-polarization	–	–
	y-polarization	–	–

As shown in Table 3, the bias-core PCF-SPR sensor proposed in this study shows remarkable advantages in two-parameter detection and successfully realizes the synchronous detection of temperature and refractive index, with the temperature detection range of 25−60 °C and the refractive index detection range of 1.31−1.40 RIU. Compared with similar sensors reported in recent years, this design has achieved excellent comprehensive performance while keeping the structure simple. The temperature sensitivity reaches 7.8 nm/°C, which is superior to most multi-parameter sensors, and the refractive index sensitivity is 28 400 nm/RIU, which still maintains competitiveness in a wider detection range. The results show that the single gold nanowire structure design adopted in this study provides a new solution for multifunctional SPR sensing, which simplifies the structure and optimizes the performance at the same time, and has important application value.

Tab. 3 Comparison of sensing performance of different PCF-SPR sensors

Sensor structure	Temperature (°C)	*RI* (RIU)	S_T (nm/°C)	S_λ (nm/RIU)	Year	Ref.
Dual symmetrical eccentric-core	–	1.13~1.35	–	17 500	2020	[27]
PCF	–	1.13~1.45	–	40 000	2023	[28]
PCF	–	1.34-1.39	–	51 200	2024	[29]
ARF	20-30	–	10.8	–	2024	[30]
PCF	0-100	1.410~1.435	6.6	29 800	2025	[31]
PCF	**25-60**	**1.31~1.40**	**7.8**	**28 400**	**2025**	**This work**

4 Conclusion

A biased-core PCF-SPR sensor based on a single gold nanowire is proposed. The fabrication process of this sensor is simple, the PCF consists of only two sizes of air holes arranged periodically, and the gold nanowire sensing structure is only formed by directly attaching the gold nanowire outside the fiber cladding. The sensing performance of the single gold nanowire bias-core PCF-SPR sensor is investigated by the finite element method. The simulation results show that the sensor can detect the refractive index of 1.31−1.40 in x-polarization mode, with the highest wavelength sensitivity of 14 800 nm/RIU, amplitude sensitivity of −1 724.25 RIU^{-1} and resolution of 6.75×10^{-6} RIU. In y-polarization mode, the detection range is 1.34−1.40, the highest wavelength sensitivity is 28 400 nm/RIU, the amplitude sensitivity is −1 289.93 RIU^{-1}, and the resolution is 3.52×10^{-6} RIU. In temperature sensing, the maximum wavelength sensitivity is 7.8 nm/°C and the maximum temperature resolution is 1.38×10^{-6} °C in the range of 25−60 °C. Finally, the sensing performance of the sensor is investigated for specific temperature sensing applications with a maximum wavelength sensitivity up to 7.8 nm/°C and a maximum temperature resolution of 1.38×10^{-6} °C. Due to its simple structure, wide detection range and high sensitivity, the sensor has great potential in biochemical detection, environmental detection and medical detection.

References:

[1] ABDELMALEK F. Study of the optical properties of corroded gold-aluminum films using surface plasmon resonances[J]. *Thin Solid Films*, 2001, 389(1-2): 296-300.

[2] BARNES W L, DEREUX A, EBBESEN T W. Surface plasmon subwavelength optics[J]. *Nature*, 2003, 424(6950): 824-830.

[3] YAN H D, LIU B, FAN G H, *et al*.. Tailoring the surface plasmon resonance energy of Au nanowire arrays by defect management and thermal treatment[J]. *Physica E: Low-dimensional Systems and Nanostructures*, 2020, 121: 114092.

[4] KELLY K L, CORONADO E, ZHAO L L, *et al*.. The optical properties of metal nanoparticles: the influence of size, shape, and dielectric environment[J]. *The Journal of Physical Chemistry B*, 2003, 107(3): 668-677.

[5] XIA Y, YANG P, SUN Y, *et al*.. One-dimensional nanostructures: synthesis, characterization, and applications[J]. *Advanced Materials*, 2003, 15(5): 353-389.

[6] MIN R, LIU ZH Y, PEREIRA L, *et al*.. Optical fiber sensing for marine environment and marine structural health monitoring: a review[J]. *Optics & Laser Technology*, 2021, 140: 107082.

[7] LEAL-JUNIOR A G, THEODOSIOU A, MIN R, *et al*.. Quasi-distributed torque and displacement sensing on a series elastic actuator's spring using FBG arrays inscribed in CYTOP fibers[J]. *IEEE Sensors Journal*, 2019, 19(11): 4054-4061.

[8] LIU Q M, DONG J, LIU J Y, *et al*.. Germanium doped D-shaped PCF-SPR methane high sensitivity sensor[J]. *Physica Scripta*, 2024, 99(11): 115512.

[9] LUAN N N, WANG R, LV W H, *et al*.. Surface plasmon resonance sensor based on D-shaped microstructured optical fiber with hollow core[J]. *Optics Express*, 2015, 23(7): 8576-8582.

[10] SARDAR R, FAISAL M. Dual-core dual-polished PCF-SPR sensor for cancer cell detection[J]. *IEEE Sensors Journal*, 2024, 24(7): 9843-9854.

[11] HASSANI A, SKOROBOGATIY M. Design of the microstructured optical fiber-based surface plasmon resonance sensors with enhanced microfluidics[J]. *Optics Express*, 2006, 14(24): 11616-11621.

[12] RIFAT A A, MAHDIRAJI G A, CHOW D M, *et al*.. Photonic crystal fiber-based surface Plasmon resonance sensor with selective analyte channels and graphene-silver deposited core[J]. *Sensors*, 2015, 15(5): 11499-11510.

[13] LIU CH, WANG F M, LV J W, *et al*.. A highly temperature-sensitive photonic crystal fiber based on surface Plasmon resonance[J]. *Optics Communications*, 2016, 359: 378-382.

[14] RIFAT A A, AHMED R, YETISEN A K, *et al*.. Photonic crystal fiber based plasmonic sensors[J]. *Sensors and Actuators B: Chemical*, 2017, 243: 311-325.

[15] LIU CH, SU W Q, WANG F M, *et al*.. Birefringent PCF-based SPR sensor for a broad range of low refractive index detection[J]. *IEEE Photonics Technology Letters*, 2018, 30(16): 1471-1474.

[16] LI H P, RUAN J, LI X, *et al*.. High-sensitivity temperature sensor based on photonic crystal fiber filled with ethanol and toluene[J]. *ECS Journal of Solid State Science and Technology*, 2023, 12(12): 127007.

[17] BING P B, HUANG SH CH, SUI J L, *et al*.. Analysis and improvement of a dual-core photonic crystal fiber sensor[J]. *Sensors*, 2018, 18(7): 2051.

[18] FALAH A A S, WONG W R, MAHDIRAJI G A, *et al*.. Single-mode D-shaped photonic crystal fiber surface plasmon resonance sensor with open microchannel[J]. *Optical Fiber Technology*, 2022, 74: 103105.

[19] DU ZH H, LIU H L. Mid-infrared refractive index photonic crystal fiber sensor based on surface plasmon resonance for ultra-high sensitivity[J]. *Laser Physics*, 2023, 33(1): 016201.

[20] 刘庆敏, 侯尚林, 雷景丽. D 型表面等离子共振光纤液体生物传感器设计与分析 (英文)[J]. 光子学报, 2022, 51(9): 0906007.
LIU Q M, HOU SH L, LEI J L. Design and analysis of D-shaped surface Plasmon resonance fiber biosensor for liquid analytes[J]. *Acta Photonica Sinica*, 2022, 51(9): 0906007.

[21] ZHOU CH. Theoretical analysis of double-microfluidic-channels photonic crystal fiber sensor based on silver nanowires[J]. *Optics Communications*, 2013, 288: 42-46.

[22] QIN J Y, MENG ZH Y, GAO J L, *et al*.. Surface plasmon enhanced polarization filter of high birefringence photonic crystal fiber with a partial core based on filled silver nanowire[J]. *Optical Fiber Technology*, 2020, 60: 102342.

[23] MESHGINQALAM B, BARVESTANI J. Highly sensitive photonic crystal fiber-based plasmonic biosensor with improved malaria detection application[J]. *The European Physical Journal Plus*, 2022, 137(5): 581.

[24] LIU Q M, DONG J, HOU SH L, *et al*.. Multi-parameter gold-film embedded PCF sensors based on surface plasmon resonance[J]. *Plasmonics*, 2024, 20(1): 93-103.
[25] SELVENDRAN S, RAJA A S, YOGALAKSHMI S. A highly sensitive surface Plasmon resonance biosensor using photonic crystal fiber filled with gold nanowire encircled by silicon lining[J]. *Optik*, 2018, 156: 112-120.
[26] LIU CH, YANG L, LIU Q, *et al*.. Analysis of a surface Plasmon resonance probe based on photonic crystal fibers for low refractive index detection[J]. *Plasmonics*, 2018, 13(3): 779-784.
[27] WANG J W, LIU CH, WANG F M, *et al*.. Surface plasmon resonance sensor based on coupling effects of dual photonic crystal fibers for low refractive indexes detection[J]. *Results in Physics*, 2020, 18: 103240.
[28] HE J, WANG J X, YANG L, *et al*.. Ring-core photonic crystal fiber sensor based on SPR for extra-wide refractive index detection[J]. *Coatings*, 2023, 13(7): 1207.
[29] LIU J Y, DONG J, LIU Q M, *et al*.. High-performance gold-nanowires-coated PCF-SPR sensor for refractive index detection[J]. *Plasmonics*, 2024, 20(6): 3753-3762.
[30] LIU M Q, LI X L, LIU W, *et al*.. ARF dual-channel magnetic field and temperature sensor based on the SPR effect[J]. *Plasmonics*, 2024, 19(5): 2729-2742.
[31] XU T F, PU SH L, HUANG S Y, *et al*.. Three-channel photonic crystal fiber sensor for simultaneous measurement of magnetic field, temperature, and refractive index[J]. *IEEE Sensors Journal*, 2025, 25(6): 9593-9599.
[32] LIU J Y, DONG J, HOU SH L, *et al*.. Design of a gold-nanowires embedded PCF for magnetic field and temperature sensing[J]. *Plasmonics*, 2025, 20(5): 2457-2466.
[33] MUMTAZ F, ZHANG B H, ROMAN M, *et al*.. Computational study: windmill-shaped multi-channel SPR sensor for simultaneous detection of multi-analyte[J]. *Measurement*, 2023, 207: 112386.
[34] LYU T T, ARCHAMBAULT C M, HATHAWAY E, *et al*.. Self-limiting sub-5 nm nanodiamonds by geochemistry-inspired synthesis[J]. *Small*, 2023, 19(33): 2300659.
[35] IBRAHIMI K M, KUMAR R, PAKHIRA W. C-grooved dual-core PCF SPR biosensor with graphene/au coating for enhanced early cancer cell detection[J]. *Applied Physics A*, 2024, 130(6): 439.
[36] AN G W, HAO X P, LI SH G, *et al*.. D-shaped photonic crystal fiber refractive index sensor based on surface plasmon resonance[J]. *Applied Optics*, 2017, 56(24): 6988-6992.
[37] LIU Y CH, LI SH G, CHEN H L, *et al*.. Surface plasmon resonance induced high sensitivity temperature and refractive index sensor based on evanescent field enhanced photonic crystal fiber[J]. *Journal of Lightwave Technology*, 2020, 38(4): 919-928.
[38] GUO Y, LI J SH, LI SH G, *et al*.. Dual-polarized optical sensing of microstructure fiber with pentagonal-lattice based on surface plasmon resonance in the near-IR spectrum[J]. *Optik*, 2020, 202: 163671.
[39] CHU S D, NAKKEERAN K, ABOBAKER A M, *et al*.. Design and analysis of surface-plasmon-resonance-based photonic quasi-crystal fiber biosensor for high-refractive-index liquid analytes[J]. *IEEE Journal of Selected Topics in Quantum Electronics*, 2019, 25(2): 6900309.
[40] MELWIN G, SENTHILNATHAN K. High sensitive D-shaped photonic crystal fiber sensor with V-groove analyte channel[J]. *Optik*, 2020, 213: 164779.
[41] LI T SH, ZHU L Q, YANG X CH, *et al*.. A refractive index sensor based on H-shaped photonic crystal fibers coated with ag-graphene layers[J]. *Sensors*, 2020, 20(3): 741.
[42] BARNES N P, PILTCH M S. Temperature-dependent Sellmeier coefficients and coherence length for cadmium telluride[J]. *Journal of the Optical Society of America*, 1977, 67(5): 628-629.

Author Biographies:

HOU Shang-lin (1970—), male, born in Qin'an, Gansu Province, Professor, he received his PhD from Beijing University of Posts and Telecommunications in 2008. He is mainly engaged in the research of new optical fiber and high-speed optical communication devices, next-generation high-speed all-optical communication networks, optical fiber sensor devices and networks. E-mail: houshanglin@vip.163.com